Temperature Coefficients of Solar Cell Parameters at Maximum Power Point

Alfredo Sanchez Garcia, Sissel Tind Kristensen,
Sjur Narten Christiansen and Rune Strandberg
University of Agder, Grimstad, 4879, Norway

Abstract

Analytical expressions for the temperature coefficients of the maximum power point voltage and current are presented. The temperature coefficients are calculated assuming the bandgap to be a linear function of the temperature and accounting for energy losses of non-radiative nature. The latter are introduced in the model through the External Radiative Efficiency. The so-called γ parameter, which has been shown to account for the thermal sensitivity of all mechanisms determining the open-circuit voltage, appears to also play a role in the temperature coefficient of the maximum power point voltage and current. Numerical results and a comparison with experimental measurements are also presented.

1 Introduction

Solar cells are generally characterized and optimized under standard test conditions (STC), defined as a global standard solar spectrum AM 1.5G, an irradiance of 1000 W/m^2, and a cell temperature of 298 K [1, 2, 3]. An increase in cell temperature results in a linear decrease in efficiency for most semiconductor materials [1, 4]. In order to optimize solar cells, it is therefore of high relevance to understand and being able to quantify the effect of changes in temperature.

The temperature sensitivity of any solar cell parameter is described by its temperature coefficient (TC) [1]. Some work has been done aiming to explicitly quantify the TCs of the open-circuit voltage, V_{oc}, and the short-circuit current, J_{sc} [2, 3], but, so far, there has not been much focus on the TCs for the maximum power point

voltage, V_{mpp} and current, J_{mpp}. In this work, we aim to find analytical expressions for the TCs of these two quantities.

This work is structured as follows: we make use of the expressions for V_{mpp} and J_{mpp}, previously derived by Sergeev and Sablon in Ref. [5], to derive analytical expressions for the respective TCs. Our approach is inspired by the work of Dupré et al. in Ref. [3] and, therefore, energy losses related to non-radiative recombination are also considered through the *External Radiative Efficiency* (ERE). The derived expressions also account for temperature variations of the bandgap, which we model as a linear function of the temperature. We discuss the limit case where only radiative recombination occurs and where the bandgap is a constant with respect to temperature variations. Additionally, we discuss how a more realistic temperature dependence of the bandgap affects the derived expressions for the TCs. Finally, we present numerical results and compare them with experimental measurements.

2 Theoretical Background

In the radiative limit and assuming non-degenerate conditions, so that we can approximate Fermi-Dirac by Maxwell-Boltzmann distributions, the total current produced by a solar cell is given by Shockley's diode equation [6],

$$J = J_{\mathrm{G}} - J_0 \exp\left(\frac{qV}{kT}\right), \tag{1}$$

where J_{G} is the *generation current* and J_0 is the *dark saturation current*. Assuming the Sun to be a black body radiating at $T_s = 6000$ K, J_{G} is given by

$$J_{\mathrm{G}} = \frac{2\pi q}{c^2 h^3} \frac{X}{X_{max}} \int_{E_g}^{\infty} \frac{E^2}{\exp\left(\frac{E}{kT_s}\right) - 1}\, dE, \tag{2}$$

with h, q, c and X being Planck's constant, the elementary charge, the speed of light and the Sun concentration factor, respectively. In the radiative limit, J_0 is given by [6]

$$J_0 = \frac{2\pi q}{c^2 h^3} \int_{E_g}^{\infty} E^2 \exp\left(-\frac{E}{kT}\right)\, dE. \tag{3}$$

2.1 Maximum Power Point

In Ref. [5], it was shown that an analytical expression for V_{mpp} can be obtained by making use of Lambert's W function, defined by $z = \mathrm{W}(ze^z)$ [7]. Consequently, an

analytical expression for J_{mpp} could be obtained by evaluating Eq. (1) at $V = V_{\mathrm{mpp}}$. The obtained expressions were

$$V_{\mathrm{mpp}} = \frac{kT}{q}\left[\mathrm{W}\left(e\frac{J_{\mathrm{G}}}{J_0}\right) - 1\right], \tag{4}$$

$$J_{\mathrm{mpp}} = J_{\mathrm{G}}\left[1 - \frac{1}{\mathrm{W}\left(e^{\frac{J_{\mathrm{G}}}{J_0}}\right)}\right]. \tag{5}$$

2.2 Temperature Coefficient

The efficiency of a solar cell varies linearly with temperature for the majority of semiconductor materials under normal operating temperatures [1]. This variation may be characterized by making use of the TC. The *relative temperature coefficient* of a photovoltaic cell parameter, X, as a function of the temperature, T, denoted here $\beta_X^r(T)$, is defined as the rate of change of X over the considered temperature range and normalized by X, i.e.,

$$\beta_{\mathrm{X}}^r(T) = \frac{1}{X(T)}\frac{\partial X}{\partial T}. \tag{6}$$

3 The Model

To account for non-radiative recombination, Green introduced the concept of External Radiative Efficiency (ERE) in Ref. [8]. The ERE is defined as *the fraction of the total dark current recombination in the cell that results in radiative emission from the cell* [8]. Admitting that the ERE may depend on the temperature, let us denote ERE $:= \mathcal{E}(T)$. Following Ref. [3], we modify Eq. (1) so that it also accounts for $\mathcal{E}(T)$ and obtain

$$J = J_{\mathrm{G}} - \frac{1}{\mathcal{E}(T)}J_0 \exp\left(\frac{qV}{kT}\right). \tag{7}$$

From Eq. (7), we can derive an expression for V_{mpp} in the same way as in Ref. [5]. In order to do so, let us first assume that the ERE is not dependent on the voltage. This is the case if, e.g., we restrict ourselves to a low-injection regime, or if we just assume carrier lifetimes which are constant with the injection level [9]. V_{mpp} then becomes

$$V_{\mathrm{mpp}} = \frac{kT}{q}\left[\mathrm{W}\left(\mathcal{E}(T)\frac{eJ_{\mathrm{G}}}{J_0}\right) - 1\right]. \tag{8}$$

3.1 Temperature Dependence of the Bandgap

Since both J_{G} and J_0 are functions of the bandgap, E_g, its temperature dependence will be important for computing the TCs. The bandgap decreases when the temperature increases for most semiconductors[1] [1]. This effect was considered in Ref. [3] by assuming a linear variation of the bandgap with the temperature, i.e.,

$$E_g(T) \approx E_{g0} + T \left. \frac{\partial E_g}{\partial T} \right|_{T=T_c}, \tag{9}$$

with E_{g0} being the bandgap at $T = 0$ K and the slope of the straight line resulting from linear fits around $T = 300$ K [4]. We will also assume that the bandgap is a linear function of the temperature and proceed to derive an expression for the TC of V_{mpp} by making use of Eq. (6).

3.2 Dark Saturation Current

Before computing the TC for V_{mpp}, let us take a look back at the dark saturation current, J_0, given in Eq. (3). Performing the integral yields:

$$J_0 = \frac{2\pi q}{c^2 h^3} kT \exp\left(-\frac{E_g}{kT}\right)(E_g^2 + 2kTE_g + 2k^2T^2). \tag{10}$$

In Ref. [3], the polynomial in E_g in Eq. (10) is approximated by E_g^2. We will refer to this as the *approximated form* of J_0, while Eq. (10) will be referred to as the *full form*. This approximated form simplified the derivation of the analytical expression for the temperature coefficient of the V_{oc}. This is also the case for V_{mpp} and J_{mpp}. In order to check the validity of this approximation, we display in Fig.1 a logarithmic plot of J_0 as a function of the temperature for the bandgap of silicon, which has been considered linear, as in Eq. (9). We see that the full and the approximated form of J_0 overlap. We will therefore make use of the approximated form of J_0 to compute the temperature coefficients of V_{mpp} and J_{mpp}. The numerical consequences of making use of this approximation will be discussed in section 5.

3.3 Temperature Coefficients

Let $Z := e\,\mathcal{E}\frac{J_{\mathrm{G}}}{J_0}$ and $\mathrm{W}(Z) := \mathrm{W}$. From Eq. (8), we have

$$\frac{\partial V_{\mathrm{mpp}}}{\partial T} = \frac{V_{\mathrm{mpp}}}{T} + \frac{kT}{q}\frac{\partial \mathrm{W}}{\partial T}. \tag{11}$$

[1]Exceptions of this behavior are $CH_3NH_3PbI_3$ and related perovskite compounds [4]

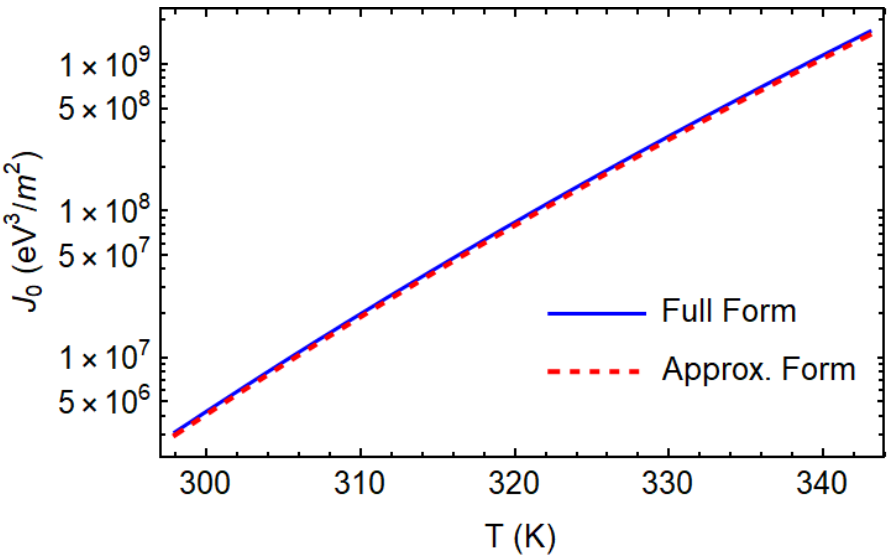

Figure 1: Dark saturation, both in full (Eq. (10)) and approximated form, as a function of the temperature.

Let us now explicitly compute the derivative of Lambert's W function with respect to the temperature. From Eqs. (3) and (9), we have

$$\begin{aligned}\frac{\partial \mathrm{W}}{\partial T} &= \frac{\partial}{\partial T}\log\left(\mathcal{E}\frac{eJ_{\mathrm{G}}}{J_0}\right)\frac{\mathrm{W}}{1+\mathrm{W}} \\ &= \left(\frac{\mathcal{E}'}{\mathcal{E}}+\frac{J'_{\mathrm{G}}}{J_{\mathrm{G}}}-\frac{J'_0}{J_0}\right)\frac{\mathrm{W}}{1+\mathrm{W}} \\ &= \left(\frac{\mathcal{E}'}{\mathcal{E}}+\frac{J'_{\mathrm{G}}}{J_{\mathrm{G}}}-\frac{1}{T}-\frac{E_{g0}}{kT^2}-2\frac{E'_g}{E_g}\right)\frac{\mathrm{W}}{1+\mathrm{W}} \\ &= -\frac{1}{T}\left(\gamma+\frac{E_{g0}}{kT}\right)\frac{\mathrm{W}}{1+\mathrm{W}},\end{aligned} \tag{12}$$

where the prime implies the derivative with respect to the temperature and

$$\gamma = 1+2T\frac{E'_g}{E_g}-T\frac{\mathcal{E}'}{\mathcal{E}}-T\frac{J'_{\mathrm{G}}}{J_{\mathrm{G}}}. \tag{13}$$

In Eq. (12), we have made use of the derivative of Lambert's W function, which can be found in, e.g., Ref. [7]. We obtain the absolute TC for V_{mpp} ($\beta_{V_{\mathrm{mpp}}}$) by

inserting Eq. (12) into Eq. (11). Let $\omega := \mathrm{W}/(1+\mathrm{W})$. We then can write $\beta_{V_{\mathrm{mpp}}}$ as

$$\beta_{V_{\mathrm{mpp}}} = \frac{V_{\mathrm{mpp}} - \omega\frac{E_{g0}}{q} - \omega\frac{kT}{q}\gamma}{T}, \tag{14}$$

which resembles the expression for $\beta_{V_{\mathrm{oc}}}$ in Ref. [3], which was

$$\beta_{V_{\mathrm{oc}}} = \frac{V_{\mathrm{oc}} - \frac{E_{g0}}{q} - \frac{kT}{q}\gamma}{T}. \tag{15}$$

The γ parameter in Eq. (13) is identical[2] to the γ used in the expression for $\beta_{V_{\mathrm{oc}}}$ in Ref. [3]. This parameter was first introduced by Green in Ref. [1] as a way to account for the temperature sensitivity of all mechanisms determining V_{oc} and was later explicitly quantified in Ref. [3]. From the work presented here, we may conclude that γ also plays a role in the temperature sensitivity of V_{mpp}.

Rearranging terms in Eq. (14), we can express $\beta_{V_{\mathrm{mpp}}}$ as

$$\beta_{V_{\mathrm{mpp}}} = \frac{V_{\mathrm{mpp}}}{T}\left[1 + \frac{\mathrm{W}}{1-\mathrm{W}^2}\left(\gamma + \frac{E_{g0}}{kT}\right)\right], \tag{16}$$

from which it is trivial to find the relative TC for $\beta_{V_{\mathrm{mpp}}}$. Likewise for J_{mpp}, we can derive expressions for its TC from Eq. (5) by making use of Eq. (6). We obtain

$$\beta_{J_{\mathrm{mpp}}} = \frac{J_{\mathrm{mpp}}}{T}\left[T\frac{J'_{\mathrm{G}}}{J_{\mathrm{G}}} + \frac{1}{1-\mathrm{W}^2}\left(\gamma + \frac{E_{g0}}{kT}\right)\right]. \tag{17}$$

3.4 The Radiative Limit with Constant Bandgap

In the radiative limit, the total current produced by the cell is given by Eq. (1). The maximum power point voltage, current and power are therefore given by Eqs. (4) and (5). All energy losses are of radiative nature and, therefore, $\mathrm{ERE} = 1$. Additionally, if the bandgap is a constant with respect to temperature variations, the γ parameter given in Eq. (13) simplifies to $\gamma = 1$. Accounting for this, Eqs. (16) and (17) become

$$\beta_{V_{\mathrm{mpp}}} = \frac{V_{\mathrm{mpp}}}{T}\left[1 + \frac{\mathrm{W}}{1-\mathrm{W}^2}\left(1 + \frac{E_{g0}}{kT}\right)\right], \tag{18}$$

$$\beta_{J_{\mathrm{mpp}}} = \frac{J_{\mathrm{mpp}}}{T}\left[\frac{1}{1-\mathrm{W}^2}\left(1 + \frac{E_{g0}}{kT}\right)\right] \tag{19}$$

[2]The notation $T\frac{X'}{X}$ is equivalent to $\frac{\partial \log X}{\partial \log T}$.

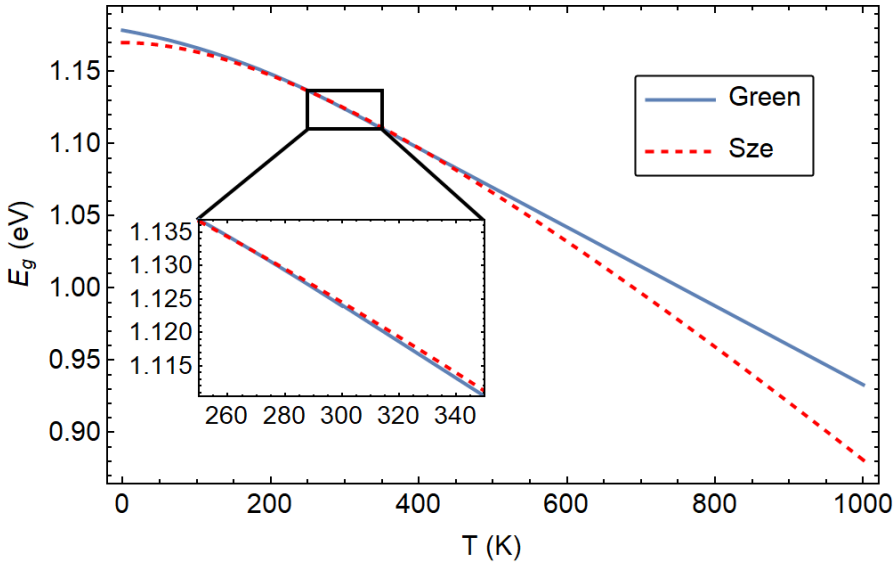

Figure 2: Temperature dependence of the energy gap, $E_g(T)$, for Green's (Eq. (9)) and Sze's (Eq. (20)) models.

3.5 A More Realistic Bandgap

In this work as well as in Ref. [3], the bandgap of silicon has been assumed to be a linear function of the temperature, as seen in Eq. (9). Sze determined in Ref. [10] the temperature dependence of E_g from the absorption edge of silicon and showed that it could be empirically described by

$$E_g(T) = E_{g0} - \frac{\alpha T^2}{T + \beta}, \tag{20}$$

where α and β are fitting parameters; and E_{g0} is the bandgap extrapolated to $T = 0$ K. Sze's model shows that at low temperatures, the bandgap has a rather quadratic dependence with the temperature, in contrasts to the linear bandgap presented in section 3.1.

Eq. (9) follows from the model for the temperature dependence of the energy gap presented by Green in Ref. [11]. There, Green modeled $E_g(T)$ as a piecewise function of the temperature, with a quadratic dependency for $T < 300$ K and a linear one for $T > 300$ K [11]. Eq. (9) represents the linear part of Green's model. Fig. 2 displays a comparison between both models. Here, we have plotted Sze's and Green's bandgap as a function of the temperature, for silicon. We see that, in the normal operating temperature range of $[300, 343]$ K, both functions overlap well.

In order to introduce Sze's bandgap in our model, we need to make use of Eq. (20) when computing J_0'. This results in one new term that should be added to the γ parameter in Eq. (13), which yields

$$\gamma = 1 + 2T\frac{E_g'}{E_g} + \frac{\alpha\beta T}{k(T+\beta)^2} - T\frac{\mathcal{E}'}{\mathcal{E}} - T\frac{J_{\mathrm{G}}'}{J_{\mathrm{G}}}. \tag{21}$$

Since we always can collect this new term into the γ parameter, the expressions for the TCs presented in this work are still valid.

Finally, as noted in Ref. [9], the deviation between Sze's and Green's models is a measure for the uncertainty of the model used. In the relevant temperature range up to 650 K, this uncertainty is below 1% and can be neglected.

4 Experimental Method

In order to validate the analytical expression for $\beta_{V_{\mathrm{mpp}}}$ and $\beta_{J_{\mathrm{mpp}}}$, 18 cells with different bulk resistivities (ρ) and cell architectures were studied. The cells were fabricated from three different compensated p-type multi-crystalline silicon (mc-Si) ingots and can be divided into three groups: (a) $\rho = 0.5\ \Omega$ cm, *Passivated Emitter Rear Cell* (PERC), (b) $\rho = 1.3\ \Omega$ cm, PERC, and (c) $\rho = 1.3\ \Omega$ cm, *Aluminum Back Surface Field* (Al-BSF) cell. Each group contains six cells from various brick positions. The $\beta_{V_{\mathrm{mpp}}}$ and $\beta_{J_{\mathrm{mpp}}}$ values were obtained from temperature dependent suns $-V_{\mathrm{oc}}$ measurements using a NeonSee$^{\mathrm{TM}}$ AAA Sun-simulator. Making use of suns $-V_{\mathrm{oc}}$ measurements allowed for TCs without the effects of series resistance.

5 Numerical Results and Discussion

In this section we present numerical results for the model presented in section 3 and compare them to experimental measurements. For all numerical evaluations, the bandgap is assumed to be a linear function of the temperature as stated in Eq. (9).

5.1 Temperature Coefficient of V_{mpp}

In Fig. 3, $\beta^r_{V_{\mathrm{mpp}}}$ is plotted as a function of V_{mpp} for $E_g' = -0.27 \times 10^{-3}$ eV K^{-1}, i.e., the temperature sensitivity of the silicon bandgap [4]. Here, Eq. (14) is represented by a dashed line and our experimental values by crosses. Note that V_{mpp} and $\beta^r_{V_{\mathrm{mpp}}}$ are increasing functions of the ERE (see Eq. (8)). The points of the dashed line in Fig. 3 are obtained by evaluating Eqs. (8) and (14) for several values of the ERE

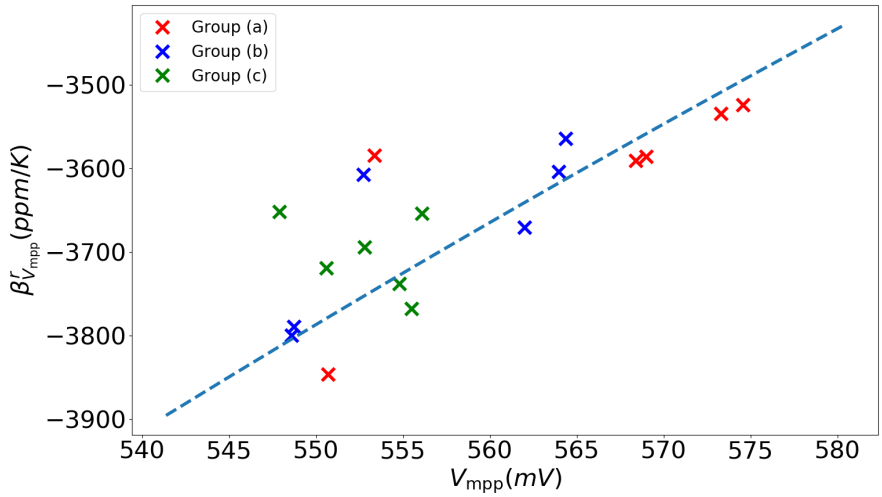

Figure 3: Relative temperature coefficient of the maximum power point voltage as a function of V_{mpp}. Eq. (14) is represented by the dashed line. The crosses represent experimental measurements of V_{mpp} of the three sets of mc-Si samples described in section IV: (a) PERC: $\rho = 0.5\ \Omega$ cm, (b) PERC: $\rho = 1.3\ \Omega$ cm and (c) Al-BSF: $\rho = 1.3\ \Omega$ cm

within the interval $\mathcal{E} \in [3,\ 15] \times 10^{-5}$. The ERE of each measurement can be calculated by subtracting the ideal and the measured V_{oc} as

$$\mathcal{E}(T) = \exp\left[\frac{q}{kT}(V_{\mathrm{oc}} - V_{\mathrm{oc}}^{\mathrm{id}})\right], \tag{22}$$

where $V_{\mathrm{oc}}^{\mathrm{id}}$ is the open-circuit voltage in the radiative limit, given in, e.g., Ref. [12]. For the samples presented in this work, we find an average value of the ERE of $\mathcal{E} = 6.99 \times 10^{-5}$. A rather low value of the ERE is expected since silicon is dominated by non-radiative recombination [1, 12]. In the light of Fig. 3, we may conclude that Eq. (14) gives food predictions of the temperature behavior of V_{mpp}.

5.2 Dark Saturation Current

As mentioned in section 3, we have been making use of the approximated form of J_0 to simplify the derivation of $\beta_{V_{\mathrm{mpp}}}$ and $\beta_{J_{\mathrm{mpp}}}$. We have numerically computed these TCs by making use of both the full and approximated form J_0 to check whether there is a significant difference. The results show a difference of 12 ppm K^{-1} at $T = 300$ K and $\mathcal{E} = 1$ up to 66 ppm K^{-1} at $T = 343$ K and $\mathcal{E} = 10^{-7}$ for $\beta^r_{V_{\mathrm{mpp}}}$ and, 0.5 ppm K^{-1} at $T = 300$ K and $\mathcal{E} = 1$ up to 10 ppm K^{-1} at $T = 343$ K and $\mathcal{E} = 10^{-7}$ for $\beta^r_{J_{\mathrm{mpp}}}$. From the measured values, as well as from Fig. 3, we see that typical values of $\beta^r_{V_{\mathrm{mpp}}}$

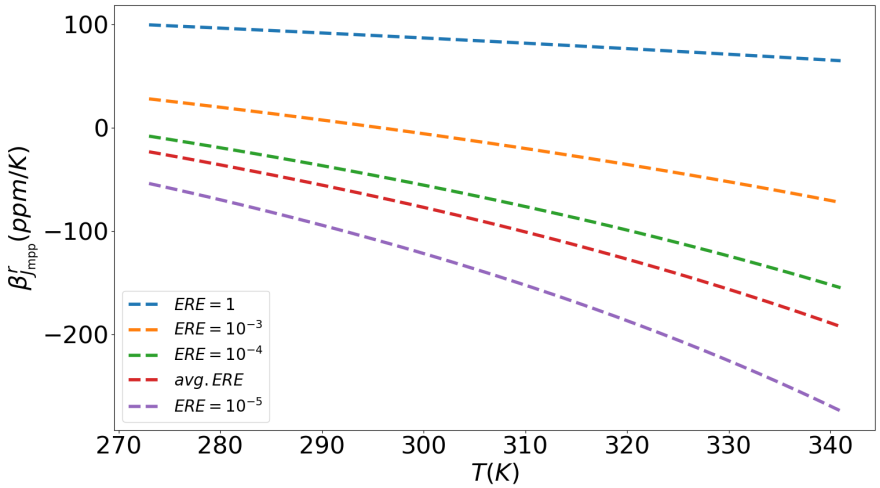

Figure 4: Relative temperature coefficient of the maximum power point current as a function of the temperature calculated from Eq. (17) for several values of the ERE.

range from -3500 to -4000 ppm K^{-1}. We can therefore conclude that having made use of the approximated form of J_0 for computing the TCs does not have significant effects in $\beta_{V_{mpp}}$ and $\beta_{J_{mpp}}$, in our cases.

5.3 Temperature Coefficient of J_{mpp}

In Fig. 4, we have plotted Eq. (17) as a function of the temperature for different values of the ERE. Here, we can see that the temperature behavior of J_{mpp} changes with a decreasing ERE. For $\mathcal{E} = 1$, $\beta^r_{J_{mpp}}(T)$ has positive values, implying that J_{mpp} increases with temperature. But when the ERE starts decreasing, we encounter negative values of $\beta^r_{J_{mpp}}(T)$, implying that J_{mpp} is decreasing with increasing temperature. Fig. 4 shows that $\beta_{J_{mpp}}$ is not a constant but rather temperature dependent, which implies J_{mpp} does not vary linearly with the temperature. Note that for $\mathcal{E} = 6.99 \times 10^{-5}$, i.e., the average ERE of our samples (sec. 5.1), we have $\beta^r_{J_{mpp}} < 0$ (red line in Fig. 4) and, particularly, $\beta^r_{J_{mpp}}(\text{avg. ERE}) = -122$ ppm K^{-1} for $T = 300$ K. Let us also note that, for $\mathcal{E} = 10^{-3}$, $\beta^r_{J_{mpp}}$ crosses zero at a temperature, denoted here T_{crit}, which equals 284 K in this specific case. $J(T_{crit})$ therefore is a maximum J_{mpp}. Note also that for $\mathcal{E} = 1$, $\beta^r_{J_{mpp}}$ is decreasing with the temperature and will eventually cross zero. Fig. 4 therefore suggests that T_{crit} is decreasing with the ERE.

Our experiments show a variety of temperature behaviors for the measured J_{mpp}. In Fig. 5, we display our measurements of J_{mpp} for three of the six investigated Al-

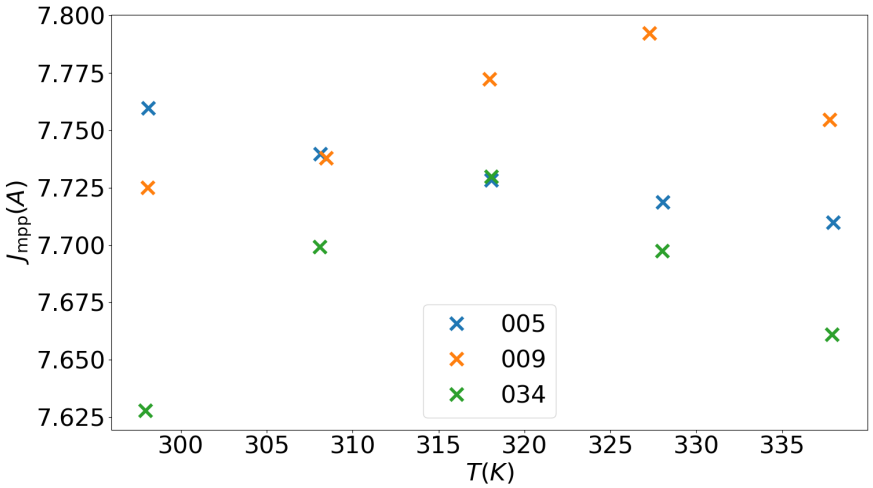

Figure 5: Measurements of J_{mpp} of the Al-BSF cell for different temperatures. Each color represents a position within the brick.

BSF cells (group (c) in sec. 4). The cells are numbered according to their position within the brick starting from the bottom, i.e., position 005 will be lower in the brick than 009. In Fig. 5, we can see that in brick position 005, J_{mpp} is clearly decreasing with the temperature. This is also the case for three other cells in positions 012, 022 and 027. These are not displayed in Fig. 5. In positions 009 and 034, J_{mpp} appears to increase with temperature, reach a maximum and then decrease. In our measurements of the PERC cells (groups (a) and (b) in sec. 4), J_{mpp} is increasing with the temperature in most brick positions. There are however a few positions where the measured values J_{mpp} vary in a non-systematic manner, and it is hard to see any increasing or decreasing trend. A similar behavior as the one found in positions 009 and 034 of group (c) is found in positions 012 and 041 of group (a).

The TC of J_{mpp} in each position is calculated by least-square fitting the measured values of J_{mpp} to a straight line. $\beta_{J_{\text{mpp}}}$ will therefore be the value of the slope. This method gives reasonable fitting errors in those brick positions where J_{mpp} shows a clear increasing, or decreasing, trend. In the case of position 005 in Fig. 5, we find $\beta^r_{J_{\text{mpp}}} = -156 \pm 16$ ppm K^{-1}. In the case of positions 009 and 034, where J_{mpp} shows both an increasing and a decreasing behavior, the fit gives $\beta^r_{J_{\text{mpp}}} = 147 \pm 96$ ppm K^{-1} and $\beta^r_{J_{\text{mpp}}} = 85 \pm 180$ ppm K^{-1}, respectively. The non-linearity of J_{mpp} originates these large uncertainties. It is therefore reasonable to conclude that making use of a single TC to describe the temperature behavior of J_{mpp} may be misleading.

Our model has limitations that may be able to explain the discrepancy with our

experiments. First, the spectral response of the solar cell. Eq. (7), assumes unit absorptivity [6]. In real solar cells, the absorption coefficients are not step-functions but rather smooth functions of the incoming wavelength which also depend on the cell temperature [13] and, therefore, they will play a role in the temperature coefficients. Particularly, the spectral response of the cell will affect the value of J'_{G}. Second, whereas our model assumes an ideality factor of 1, the IV-curve of real cells are often better described by a larger ideality factor [14]. A temperature dependent ideality factor, $n(T)$, will possibly also affect the TCs.

These two factors may not be sufficient to explain the discrepancies, so let us focus now on the experiments. The biggest source of uncertainty in our measurements comes from the difficulty in stabilizing the temperature during the relatively long data-acquisition times. This results in not only uncertainty in the temperature, but possibly also in the measured values of V_{mpp} and J_{mpp}. The uncertainty of the temperature propagates in the calculation of the TCs further increasing the fitting errors. Within the investigated temperature range, $\beta_{J_{\mathrm{mpp}}}$ varies with temperature (see Fig. 4) while $\beta_{V_{\mathrm{mpp}}}$ is nearly constant. Small temperature fluctuations will therefore cause a bigger, and significant, effect on $\beta_{J_{\mathrm{mpp}}}$ than on $\beta_{V_{\mathrm{mpp}}}$.

Finally, T_{crit} may be the last piece of the puzzle to explain the discrepancies between Eq. (17) and our experiments. A T_{crit} dependent on the brick position and the cell architecture may explain the variety of temperature behaviors that our experiments show. J_{mpp} has not reached T_{crit} in the cells that show an only increasing J_{mpp}. At the same time, those cells only showing a decreasing J_{mpp} have a T_{crit} lower than the temperature range in which the measurements were performed, as seen, for example, in Fig. 5 in the measurements of the cell from position 005. Finally, the positions where J_{mpp} first increases and then decreases with the cell temperature reach their correspondent T_{crit} within the investigated temperature range. This is the case for brick positions 009 and 034 in Fig. 5, where we can see that their correspondent T_{crit} is around 328 K and 318 K, respectively.

6 Conclusion

In this paper, we have presented analytical expressions for the TCs of V_{mpp} and J_{mpp}. It was discussed in Ref. [3] that the γ parameter, first introduced in Ref. [1], accounts for the temperature sensitivity of all mechanisms determining the V_{oc}. From the results presented in section 3, we conclude that γ may also determine the thermal sensitivity of V_{mpp} and J_{mpp}.

Numerical results as well as a comparison with experimental measurements of $\beta_{V_{\mathrm{mpp}}}$ and $\beta_{J_{\mathrm{mpp}}}$ have also been presented and discussed. We have found that our

model gives good predictions of the temperature behavior of the measured values of $\beta_{V_{\mathrm{mpp}}}$. The mismatch between the experimental measurements of $\beta_{J_{\mathrm{mpp}}}$ and Eq. (17) suggests that there are one or more factors, which are not accounted for in our model, that affect the temperature sensitivity of J_{mpp}. The solar cell spectral response and a temperature dependent ideality factor have been proposed as possible explanations to the discrepancy. The uncertainty of the measurements due to small temperature fluctuations may also contribute to the discrepancy between the experiments and Eq. (17). Finally, Fig. 4 shows that $\beta_{J_{\mathrm{mpp}}}$ is not a constant within the investigated temperature range. Additionally, it can be seen in Fig. 4 that $\beta_{J_{\mathrm{mpp}}}(T)$ crosses zero at an ERE-dependent critical temperature, implying that J_{mpp} reaches a maximum at this temperature.

References

[1] M. A. Green. "Solar cells: operating principles, technology, and system applications". In: *Englewood Cliffs, NJ, Prentice-Hall, Inc., 1982. 288 p.* (1982).

[2] M. A. Green. "General temperature dependence of solar cell performance and implications for device modeling". In: *Progress in Photovoltaics: Research and Applications* 11.5 (2003), pp. 333–340.

[3] O. Dupré, R. Vaillon, and M. A. Green. "Physics of the temperature coefficients of solar cells". In: *Solar Energy Materials and Solar Cells* 140 (2015), pp. 92–100.

[4] O. Dupré, R. Vaillon, and M. A. Green. *Thermal Behavior of Photovoltaic Devices: Physics and Engineering*. Springer, 2016.

[5] A. Sergeev and K. Sablon. "Exact solution, endoreversible thermodynamics, and kinetics of the generalized Shockley-Queisser model". In: *Physical Review Applied* 10.6 (2018), p. 064001.

[6] W. Shockley and H. J. Queisser. "Detailed balance limit of efficiency of p-n junction solar cells". In: *Journal of Applied Physics* 32.3 (1961), pp. 510–519.

[7] R. M. Corless et al. "On the Lambert W function". In: *Advances in Computational Mathematics* 5.1 (1996), pp. 329–359.

[8] M. A. Green. "Radiative efficiency of state-of-the-art photovoltaic cells". In: *Progress in Photovoltaics: Research and Applications* 20.4 (2012), pp. 472–476.

[9] S. Rein. *Lifetime Spectroscopy: A Method of Defect Characterization in Silicon for Photovoltaic Applications*. Vol. 85. Springer Science & Business Media, 2006.

[10] S. M. Sze. "Physics of Semiconductor Devices 2nd edition Awiley Inter-science John wiley and Sons". In: *New York* (1981).

[11] M. A. Green. "Intrinsic concentration, effective densities of states, and effective mass in silicon". In: *Journal of Applied Physics* 67.6 (1990), pp. 2944–2954.

[12] J. Nelson. *The Physics of Solar Cells*. World Scientific Publishing Company, 2003.

[13] K. Rajkanan, R. Singh, and J. Shewchun. "Absorption coefficient of silicon for solar cell calculations". In: *Solid-State Electronics* 22.9 (1979), pp. 793–795.

[14] A. McEvoy and T. Markvart. *Solar cells: materials, manufacture and operation*. Academic Press, 2012.